

Omnidirectional Depth-Aided Occupancy Prediction based on Cylindrical Voxel for Autonomous Driving

Chaofan Wu^{*1}, Jiaheng Li^{*1}, Jinghao Cao¹, Ming Li¹, Yongkang Feng¹, Jiayu Wu¹
Shuwen Xu¹, Zihang Gao¹, Sidan Du^{✉1}, Yang Li^{✉1,2}

Abstract—Accurate 3D perception is essential for autonomous driving. Traditional methods often struggle with geometric ambiguity due to a lack of geometric prior. To address these challenges, we use omnidirectional depth estimation to introduce geometric prior. Based on the depth information, we propose a Sketch-Coloring framework OmniDepth-Occ. Additionally, our approach introduces a cylindrical voxel representation based on polar coordinate to better align with the radial nature of panoramic camera views. To address the lack of fisheye camera dataset in autonomous driving tasks, we also build a virtual scene dataset with six fisheye cameras, and the data volume has reached twice that of SemanticKITTI. Experimental results demonstrate that our Sketch-Coloring network significantly enhances 3D perception performance.

I. INTRODUCTION

Accurate perception of the surrounding environment is crucial for autonomous driving system. In recent years, vision-based 3D perception algorithms have gained significant attention and advancement. The typical workflow involves employing a 2D encoder to extract latent representations from images and a view transformation method [1].

The methods for view transformation mainly fall into two categories, as shown in Fig.1. The first involves using explicit depth estimation to elevate 2D features from images into a 3D voxel space [2], [3], [4], [5]. However, this method is difficult to reconstruct occluded regions and thus producing suboptimal results. The second category is based on transformer architecture. Spatial-Cross-Attention (SCA) is used to extract 3D features from the images [6], [7], [8]. However, transformer-based methods rely solely on attention mechanism for perspective transformation without any geometric prior. This makes it challenging to distinguish between image regions and the spatial relationship of real-world objects [6], leading to a heavy dependence on large datasets. To address these limitations, using depth estimation result to constrain the transformer is necessary.

Moreover, traditional occupancy (Occ) schemes typically use multiple pinhole cameras mounted around the vehicle. Due to the limited field of view (FOV) of pinhole cameras, the overlapping regions between adjacent views are usually very small. In this scenario, the process of extracting depth information from images tends to rely on monocular depth estimation, which is an ill-posed problem. The accuracy of monocular depth estimation is significantly inferior to that of omnidirectional depth estimation with more overlapping

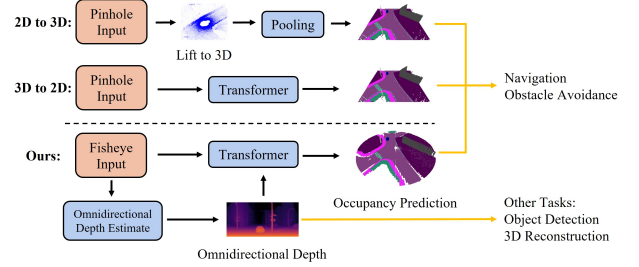


Fig. 1. The typical workflow of occupancy prediction & our Sketch-Coloring framework.

regions [9], severely impacting the effectiveness of scene completion.

Currently, most occupancy prediction methods are based on the Cartesian coordinate system, where space is uniformly divided to obtain a cuboid voxel grid. Each voxel contains both occupancy and semantic information. However, we have identified several issues with this voxel-based approach:

- **A mismatch between voxel resolution and prediction accuracy.** All voxels are the same size, but in practice, voxels closer to the ego vehicle have higher semantic confidence than those farther away. In this context, the prediction accuracy for nearby regions is constrained by voxel resolution, while prediction error for distant regions often exceeds the size of the voxels. This leads to results that do not accurately represent the real-world scene.
- **A mismatch between the perception field and surround-view cameras.** For instance, consider two voxels, v_a and v_b , which are equidistant from the ego vehicle. But v_a is within the voxel grid and v_b is outside it, as illustrated in Fig.2(a). For the input image, v_a and v_b have the same weight (they share the same depth). But only the features of v_a will contribute to the loss function, while v_b will not, which hinders network convergence.
- **Unreasonable voxel density allocation.** For a moving vehicle, nearby objects are more crucial to monitor than distant ones since they pose a greater immediate threat. Downstream tasks like obstacle avoidance and navigation should focus on nearby objects. Thus, a 3D spatial representation for autonomous driving should be denser in nearby regions to align with the practical needs of autonomous driving scenarios.

Motivated by the aforementioned insights, we propose a

*: Equal Contribution

✉: Corresponding Author

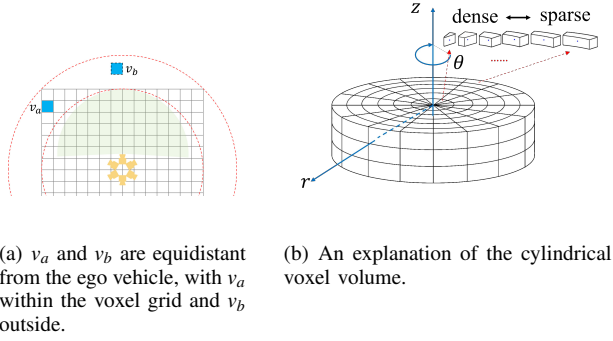


Fig. 2. Two instances to illustrate the characteristic of Cartesian and Cylinder coordinate system.

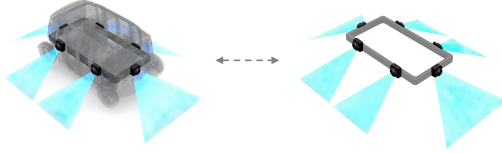


Fig. 3. The distribution of cameras on our unmanned vehicle.

Sketch-Coloring framework for occupancy prediction tasks in a polar coordinate system using multiple fisheye cameras. We design a cylindrical voxel grid, as shown in Fig.2(b), which is more suitable and natural for occupancy prediction tasks compared to Cartesian coordinate system. In fact, some lidar-based 3D object detection methods have already leveraged the polar coordinate [10], [11], [12], [13], [14]. Our method leverages depth estimation to predict approximate geometric information, leading to higher accuracy in occupancy prediction. By leveraging fisheye cameras' overlapping regions, this approach boosts depth estimation accuracy and enhances scene completion performance. We used an unmanned vehicle equipped with six fisheye cameras to validate our method in a virtual environment. The specific camera distribution is shown in Fig.3. It should be noted that the distribution of our cameras can be flexibly adjusted according to requirements.

Our contributions are as follows.

- 1) **A Sketch-Coloring network structure based on depth estimation prior.** Leveraging larger overlapping regions between fisheye cameras can greatly improve depth estimation accuracy and provide precise structural information for the Sketch-Coloring network. The experimental results show a significant improvement with our method.
- 2) **A cylindrical voxel representation inspired by the polar coordinate to boost prediction performance.** This representation adjusts the density of the voxel on the basis of distance. It better aligns with surround-view cameras' distribution characteristics and enhances prediction performance.
- 3) **A virtual scene dataset with six fisheye cameras.** To address the lack of fisheye camera data in autonomous driving tasks, we developed a virtual scene dataset using six fisheye cameras.

II. RELATED WORK

A. Occupancy Datasets

Data Modality. Most current Occ datasets such as SemanticKITTI [15], Occ3D [16] and OpenOccupancy [17] have RGB inputs in the form of pinhole, and the semantic truth values are usually composed of cuboid semantic voxels. There are few occupancy prediction datasets that include fisheye images with large FOV, and our dataset provides a novel surround-view fisheye RGB input modality.

Acquisition Method. At present, there are two main ways to collect SSC datasets for autonomous driving scenarios: 1) Collecting data in real driving scenarios requires the construction of a complete hardware system, and the post-processing costs high, just as SemanticKITTI [15], Occ3D [16]; 2) Collecting data in simulation scenarios has the advantages of free configuration of sensors and easier post-processing, just as Paris-CARLA-3D [18], CarlaSC [19].

B. 3D Scene Representation

BEV. The past several years have witnessed the prosperous development of BEV representation in tasks such as 3D object detection [20], [21], [2], [5], [22], [23], BEV semantic segmentation [24], [25], [26]. Despite efficiency, the geometry lossy projection results in the relatively coarse representation of the 3D scene, hindering its generalization to the fine-grained semantic occupancy prediction task.

Cartesian Coordinate. Representing the surrounding environment with spatial latent information is a trend for autonomous driving perception algorithms. A direct approach is dividing the scene into a cuboid voxel grid of size (H, W, Z) in Cartesian coordinate, as seen in methods [27], [28], [29], [30], [31], [32], [7], [33], [34]. Similarly, in LiDAR point cloud segmentation tasks, the point cloud is often divided into a cuboid voxel grid for subsequent feature encoding and decoding [17], [35], [36], [37].

Polar Coordinate. In LiDAR-based perception methods, polar or quasi-polar coordinate systems have been explored for 3D object detection. For example, Cylinder3D [13] proposes a polar coordinate-based segmentation method for LiDAR point clouds. PointOcc [38] introduces a cylindrical coordinate-based tri-view representation of point clouds. In vision-based perception methods, PolarDETR [11] presents polar parameterization for 3D detection and reformulates position parameterization.

C. Vision-Based Occupancy Prediction

Occupancy prediction networks focus on reconstructing voxel-level 3D scene and predicting voxel-level semantic information from input images. MonoScene [27] achieves scene occupancy completion through a 2D and a 3D UNet connected by a sight projection module. OccNet [7] applies universal occupancy features to various downstream tasks and introduces the OpenOcc benchmark. To address the computational burden of handling a large number of voxel queries, TPVFormer [8] proposes using tri-perspective

view representation to supplement vertical structural information, though this inevitably leads to information loss. VoxFormer [6] initializes sparse queries based on stereo depth prediction. Several methods emerged in the CVPR 2023 occupancy challenge [39], [40], [41], [42], but none explored voxel representation in polar coordinate or leveraged panoramic depth estimation to introduce geometric prior.

III. VIRTUAL SCENE OCC DATASET WITH FISHEYE CAMERA INPUT

To collect an occupancy dataset from fisheye cameras, we build a simulation data collection system based on the open-source autonomous driving simulator Carla Simulator [43]. This system collects multi-view RGB images and semantic label ground truth. The distinctions of this dataset from other occupancy datasets are shown in Table I.

TABLE I
COMPARE AGAINST CLASSIC OCC DATASETS

method	pinhole images	fisheye images	cuboid voxels	polar voxels	2D semantic & depth	frames
SemanticKITTI [15]	✓		✓			23,201
Occ3D-nuScenes [16]	✓		✓			40,000
CarlaSC [19]	✓		✓	✓		43,200
Ours	✓	✓	✓	✓	✓	57,600

Inspired by CarlaSC [19], our dataset collection utilizes Carla Simulator to run a virtual driving scene in UE4 and collect data by various sensors.

It is worth mentioning that we collect cubemap images and post-process them into fisheye images. We place 20 semantic LiDARs around the vehicle and aggregate the semantic point clouds collected by all semantic LiDARs in each frame to obtain a complete semantic point cloud. We then sample this point cloud with voxel grid (both cuboid and cylindrical), then each voxel’s semantic label is determined by voting among the semantic points within it.

From the perspective of scene collection, We have collected 32 scenes under various weather conditions across 8 different maps, capturing 1800 frames per scene at a frame rate of 10 FPS. In total, the dataset comprises 57,600 frames of data. Our dataset encompasses a variety of scene conditions, including sunny, rainy, and overcast skies, and is twice the size of Semantic KITTI [15]. If our paper is accepted, we will open-source our dataset to the community.

IV. METHODOLOGY

A. Overall Architecture

As shown in Fig.4, our method consists of six main components: Image Backbone, Cylinder Sketch Module, 2D Semantic Head, Coloring Module, Temporal Fusion, and Refine Module. The Cylinder Sketch Module predicts a cylindrical, class-agnostic occupancy grid using omnidirectional depth estimation, akin to sketching. The Coloring Module uses a transformer to map image features onto the cylindrical voxel grid, akin to coloring. The 2D Semantic Head performs semantic segmentation to enhance the backbone’s semantic learning. Temporal Fusion combines temporal information

from multi-frame inputs, and the Refine Module further refines voxel features. Each component is detailed in the following sections.

B. Cylinder Sketch Module

Omnidirectional Depth Estimation. For omnidirectional depth estimation, we employ RtHexa-OmniMVS [44]. RtHexa-OmniMVS projects the feature maps from fisheye images onto N spherical surfaces with varying radius, then the matching cost is calculated to estimate depth. The obtained spherical depth is transformed to ERP (Equirectangular Projection) depth image. Then we utilize the camera’s intrinsic and extrinsic parameters to convert the ERP depth map into a pseudo-point cloud.

Cylinder Sketch. Methods based on transformers often struggle with convergence due to a lack of geometric constraints. To address this, we design the Cylinder Sketch Module to predict a sparse set of candidate voxels, which participate in the query process, to save memory. This approach is like sketching an outline. We divide the pseudo point cloud from depth estimation into cylindrical voxels and use the Cylinder3D [13] framework for candidate prediction. Additionally, we dilate along the cylindrical sketch’s radius to reduce depth estimation blurriness in distant regions, considering voxels near an occupied one within the dilation window as occupied. This dilation method is like the dilation operation in image processing.

Fig.5 illustrates the dilation process with a dilation window of 2. We set different dilation window for different distance ranges, with larger dilation window for farther regions, as shown in Fig.5(a).

C. Coloring Module

We design a Coloring Module to infuse the sketch with semantic features, akin to coloring a sketch. This module primarily consists of a cross attention structure, where we use the Cylinder Sketch as candidate query voxels. Specifically, we locate the corresponding 2D reference points of the candidate voxels by camera’s intrinsic and extrinsic parameters. These points serve as reference points for Deformable Cross Attention (as in DETR [45]). The formula for Coloring Module(CM) is as follows:

$$CM(q_c, F) = \frac{1}{H} \sum_{i \in H} DA(q_c, P(p, T_i), F_i) \quad (1)$$

Here, DA is the Deformable Attention module, q_c is the query corresponding to the candidate voxel, F is the image feature, and $P(p, T_i)$ represents the normalized pixel coordinate in the image obtained based on the voxel position and camera parameters. H includes all the feature maps that the candidate voxels hit when projected onto the image features. This process effectively lifts 2D features into 3D features, improving computational efficiency and feature representation accuracy.

Due to their wide field of view, fisheye cameras introduce significant radial and tangential distortions. To address these

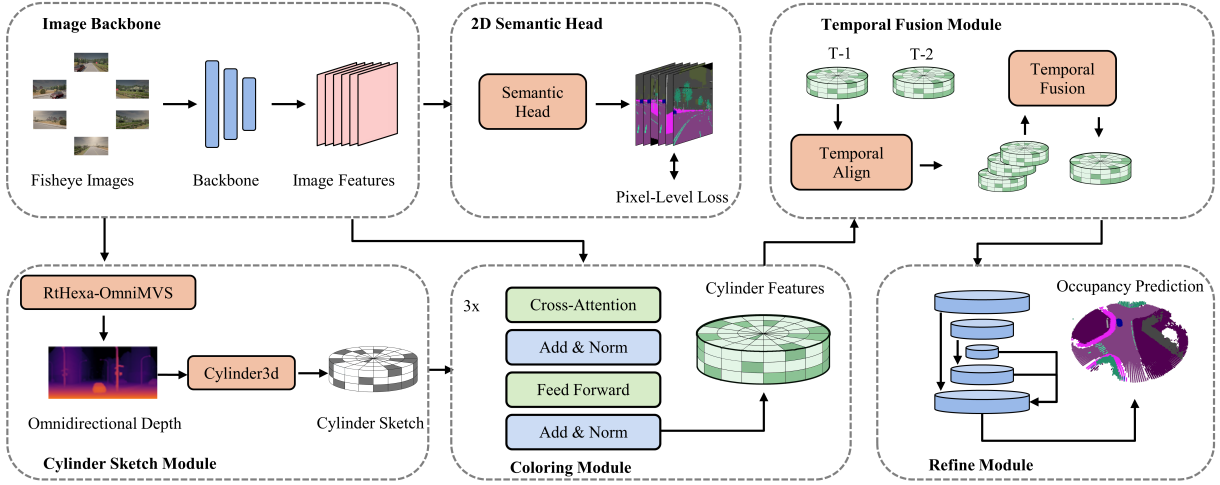
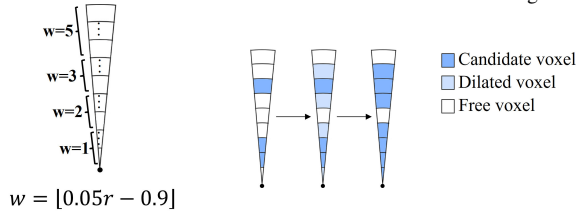


Fig. 4. Overall architecture



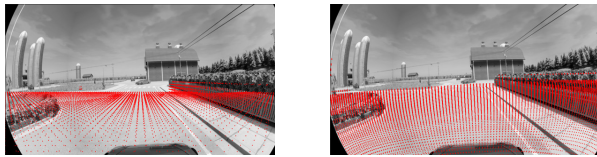
(a) Dilation window varying with distance. (b) An example to illustrate the dilation process when the dilation window is 2.

Fig. 5. The dilation process after the Cylinder Sketch Module

distortions, we apply the projection method specifically designed for fisheye image inputs and introduce Deformable Convolutional Networks(DCN) in image backbone.

In summary, by performing feature transformation only on the candidate region, we significantly reduce the computational load while ensuring accuracy. Additionally, the projection method tailored for fisheye camera distortions ensures the accuracy of feature mapping in a wide field of view.

D. 2D Semantic Head



(a) The projection of cuboid voxels. (b) The projection of cylindrical voxels.

Fig. 6. The projection of candidate voxels in the input image reflects the sparsity and imbalance of projection points. The red dots indicate the projection locations of the voxels.

In a typical occupancy task, the supervision is applied to the output voxel grid, where each voxel aggregates 3D information from the corresponding 2D pixels of multiple view images. The loss is calculated between these voxels and the ground truth, which we refer to as voxel-level supervision. We identify two issues that arise from relying solely on voxel-level supervision:

- **Indirect Supervision on Images:** The loss directly affects the voxel features. After 3D-to-2D projection and image feature sampling, the loss becomes indirect.
- **Sparse Supervision on Image Features:** Since our queries originate from occupancy prediction and are inherently sparse, this sparsity persists through the 3D-to-2D projection. As shown in Fig.6, only the sparse pixels around the 2D reference points receive a supervision signal, resulting in a decline in prediction accuracy.

Due to these reasons, the sparse voxel-level supervision on image features fails to adequately guide the backbone encoding these features. To address this, we design a semantic segmentation head applied to the image feature backbone. The segmentation head predicts per-pixel semantic labels to calculate the loss, providing richer signals for supervision.

E. Temporal Fusion

As static images without temporal cues struggle to infer the speed of moving objects or detect highly occluded objects. Therefore, we design a temporal fusion module for 3D voxel queries to further enhance voxel representations.

The temporal fusion module integrates historical voxel query information into the current voxel grid V_{curr} . As shown in Fig.4, before performing temporal fusion, voxel alignment is crucial for accurately perceiving the environment, which is formulated as follows:

$$V_{\text{fusion}} = \frac{1}{N+1} (V_{\text{curr}} + \sum_{i=1}^N \text{GS}(V_i, T_i, T_{\text{curr}})) \quad (2)$$

Here, N denotes the number of frames to be fused, V_{curr} is the current frame's voxel features extracted through Coloring Module, and $\text{GS}(V_i, T_i, T_{\text{curr}})$ represents the historical voxel features obtained using the transformation matrix between the current and historical frames followed by grid sampling.

F. Refine Module

Following the Coloring Module, we design a refine module, which is a UNet-like encoder-decoder network. After the initial voxel features are extracted by the Coloring Module, the refine module further refines these voxel features. At this

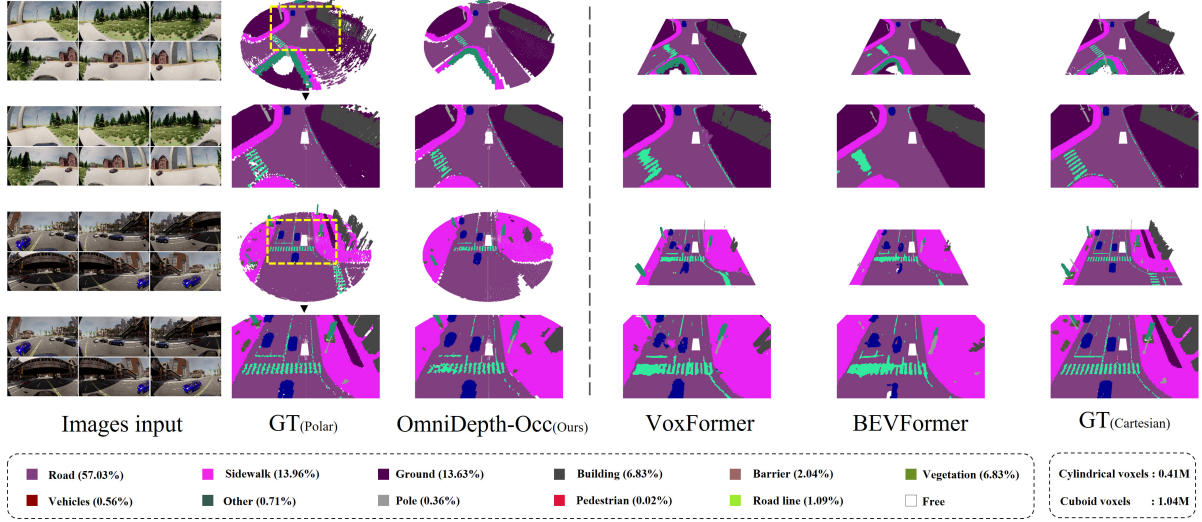


Fig. 7. Visualization results

stage, the feature extraction is not limited to the candidate voxels but applies to the entire voxel grid. This module plays a vital role in reconstructing detail and leverages the spatial consistency of voxel semantics while reducing noise.

G. Training Loss

In this paper, the sum of four loss functions is employed as the overall loss function for training purposes, as shown in Eq.3.

$$Loss = L_{CE} + L_{scal} + L_{dice} + L_{2Dsem} \quad (3)$$

Where L_{CE} denotes the weighted cross-entropy function, the weight for each class can be derived from Eq.4. L_{scal} is inspired by [27], used to mitigate the influence of class imbalance during training.

$$\omega_c = \frac{1}{\log(f_c + c)} \quad (4)$$

As shown in Eq.5, L_{dice} serving as a loss function frequently utilized in image segmentation tasks.

$$L_{dice} = 1 - \frac{2TP}{2TP + FP + FN} \quad (5)$$

The merit of Dice Loss lies in its direct optimization of the F1 score, thereby adeptly tackling extreme cases of class imbalance.

V. EXPERIMENT

A. Experimental Setup

Our Fisheye Dataset. Based on the proposed six-fisheye camera dataset, we conduct subsequent experiments. The semantic ground truth is in the form of cylindrical coordinate voxels with a shape of $(128 \times 200 \times 16)$, representing (r, θ, z) in the cylindrical coordinate. We set the perception radius within $(0m, 25.6m)$ and the height range within $(-2.8m, 3.6m)$. In terms of data augmentation, we

primarily perform random cropping on the input RGB images to enhance robustness against occlusion.

Evaluation Metrics. Our evaluation metric follows the *RayIoU* proposed in [46]. It is calculated by projecting query rays into the predicted 3D occupancy volume and ground truth separately. For each query ray, we compute the distance it travels before intersecting any surface and retrieve the corresponding class label to determine whether the prediction matches the ground truth. *RayIoU* provides a better evaluation in the presence of object occlusions and does not require annotation of the effective region of the camera. The final *RayIoU* calculation is given by Equation 6, where C is the total number of classes:

$$RayIoU = \frac{1}{C} \sum_{c=1}^C \frac{TP_c}{TP_c + FP_c + FN_c} \quad (6)$$

Here, TP refers to the cases where the predicted label matches the true label, and the difference in distance between them is within a specified threshold.

Implementation Details. For panoramic depth estimation, we employ RtHexa-OmniMVS, which generate panoramic depth maps. Our Cylinder Sketch Module is inspired by Cylinder3D [13], a highly efficient LiDAR semantic segmentation network. We train Cylinder3D for 30 epochs on 4 NVIDIA 3090 GPUs. We employ a ResNet-50 backbone with DCN as image backbone. The extracted features are fed into an FPN to aggregate multi-scale image features. The Coloring Module utilizes a Cross-Attention structure with a feature dimension of $d = 128$ for the query. For the temporal fusion module, we choose the three frames preceding the current frame. The voxel features after temporal fusion are fed into the refine module. Subsequently, a linear layer compresses the output feature dimension to 12, corresponding to the total number of classes. We train the model for 40 epochs on 4 NVIDIA 3090 GPUs, with a learning rate of 2×10^{-4} .

TABLE II
QUANTITATIVE COMPARISON AGAINST CAMERA-BASED METHODS

method	Voxels	RayIoU	Road	Sidewalk	Ground	Building	Wall	Vegetation	Vehicles	Other	Pole	Pedestrian	Roadline
BEVDet [3]	1.04M	0.310	0.714	0.608	0.505	0.141	0.203	0.095	0.367	0.120	0.113	0.007	0.235
BEVFormer [20]	1.04M	0.301	0.723	0.685	0.518	0.140	0.259	0.137	0.354	0.125	0.142	0.000	0.225
VoxFormer [6]	1.04M	0.388	0.805	0.718	0.258	0.213	0.339	0.226	0.447	0.287	0.326	0.338	0.308
OmniDepth-Occ(ours)	0.41M	0.470	0.813	0.793	0.606	0.237	0.417	0.373	0.556	0.306	0.368	0.317	0.380

TABLE III
RESULT IN DIFFERENT DISTANCE

method	RayIoU _{0-8.5m}	RayIoU _{8.5-17m}	RayIoU _{17-25.6m}
BEVDet	0.435	0.321	0.150
BEVFormer	0.421	0.319	0.177
VoxFormer	0.454	0.413	0.285
OmniDepth-Occ(ours)	0.496	0.446	0.294

TABLE IV
ABLATION STUDY FOR SEMANTIC HEAD & TEMPORAL FUSION

method	RayIoU
ours	0.470
w/o 2D semantic head	0.443
w/o temporal fusion	0.458

B. Occupancy Prediction Result

In Table II, we present the quantitative results on our validation set. All methods use only camera input and are trained for 40 epochs. Since VoxFormer [6] typically uses monocular or stereo depth along with single-view images, we extend it to a panoramic input and retrain it on our pinhole data. These methods all employ the same backbone ResNet-50.

Our method shows a 21% improvement compared to VoxFormer, a 56% improvement compared to BEVFormer, and a 51.6% improvement compared to BEVDet. Furthermore, we conduct a quantitative evaluation over different distance ranges, as shown in Table III. In comparison to VoxFormer, our model has realized more significant advancements in near-field performance, a benefit we ascribe to the augmented resolution in proximate ranges coupled with more precise depth estimation. As illustrated in Figure 7, compared to other classic methods, our method achieves finer scene reconstruction at all ranges and more accurately reconstructs dynamic objects, such as moving vehicles, with minimal trailing artifact (0.447-0.556). The overall performance is significantly enhanced.

TABLE V
ABLATION STUDY FOR REFINE MODULE

method	RayIoU
our refine module	0.470
self-attention	0.456
w/o refine module	0.391

C. Ablation Study

Ablation studies on temporal fusion and joint semantic supervision are presented in Table IV. Compared to the case of using only the current frame input, our strategy of fusing

TABLE VI
ABLATION STUDY FOR CYLINDER SKETCH MODULE

method	RayIoU
omni depth	0.470
omni depth w/o dilation	0.465
mono depth	0.263
dense voxels	0.434
random voxels	0.401

TABLE VII
ABLATION STUDY FOR CYLINDRICAL VOXEL REPRESENTATION

method	RayIoU
cylindrical voxel representation	0.454
cuboid voxel representation	0.388

three historical frames improves the mIoU by 2.6%(0.458-0.470). Compared to the case without 2D semantic supervision, our structure improves the mIoU by 6% (0.443-0.470).

Refine module ablation studies are presented in Table V. Our structure shows an 3% improvement (0.456-0.470) over the self-attention structure from VoxFormer, and improves the mIoU by 20% (0.391-0.470) compared to the method without refine module. Cylinder sketch module ablation studies are presented in Table VI. Results show that our cylinder sketch module, based on panoramic depth estimation, achieves a 78% improvement (0.263-0.470) compared to inputs using monocular depth estimation. It also shows an 8.2% improvement (0.434-0.470) over fully dense voxels and a 17.2% improvement (0.401-0.470) compared to randomly distributed voxels (with a candidate voxel ratio of 25%). Additionally, our dilation operation contributes to a slight enhancement in the results (0.465-0.470).

We conducted ablation experiments on the cylindrical voxel representation, with the results presented in Table VII. During the experiments, the refine module and temporal fusion module were removed, and only the effect of replacing square voxels with cylindrical voxels was observed. The experimental results indicate that the predicted RayIoU increased from 0.388 to 0.454(17.0%).

VI. CONCLUSION

In summary, we present OmniDepth-Occ, a cylindrical voxel-based Sketch-Coloring framework. It uses omnidirectional depth estimation to constrain transformer. Additionally, we propose a polar coordinate-based cylindrical voxel representation and a virtual scene dataset with six fisheye cameras for our network. Experimental results demonstrate that our OmniDepth-Occ achieves a significant accuracy improvement especially in close range, surpassing classical methods like VoxFormer and BEVFormer. Our system not

only generates occupancy prediction for navigation and obstacle avoidance, but also provides dense depth information that can offer sufficient structural information for more tasks such as 3D reconstruction and object detection. These will be further explored in our future work.

REFERENCES

- [1] Hongyang Li, Chonghao Sima, Jifeng Dai, Wenhai Wang, Lewei Lu, Huijie Wang, Jia Zeng, Zhiqi Li, Jiazhi Yang, Hanming Deng, Hao Tian, Enze Xie, Jiangwei Xie, Li Chen, Tianyu Li, Yang Li, Yulu Gao, Xiaosong Jia, Si Liu, Jianping Shi, Dahua Lin, and Yu Qiao. Delving into the devils of bird's-eye-view perception: A review, evaluation and recipe. *IEEE Transactions on Pattern Analysis and Machine Intelligence*, pages 1–20, 2023.
- [2] Jonah Philion and Sanja Fidler. Lift, splat, shoot: Encoding images from arbitrary camera rigs by implicitly unprojecting to 3d. In *Proceedings of the European Conference on Computer Vision*, 2020.
- [3] Junjie Huang, Guan Huang, Zheng Zhu, Ye Yun, and Dalong Du. Bevdet: High-performance multi-camera 3d object detection in bird-eye-view. *arXiv preprint arXiv:2112.11790*, 2021.
- [4] Junjie Huang and Guan Huang. Bevdet4d: Exploit temporal cues in multi-camera 3d object detection. *arXiv preprint arXiv:2203.17054*, 2022.
- [5] Yinhao Li, Zheng Ge, Guanyi Yu, Jinrong Yang, Zengran Wang, Yukang Shi, Jianjian Sun, and Zeming Li. Bevdepth: Acquisition of reliable depth for multi-view 3d object detection. *arXiv preprint arXiv:2206.10092*, 2022.
- [6] Yiming Li, Zhiding Yu, Christopher Choy, Chaowei Xiao, Jose M Alvarez, Sanja Fidler, Chen Feng, and Anima Anandkumar. Voxformer: Sparse voxel transformer for camera-based 3d semantic scene completion. In *Proceedings of the IEEE/CVF Conference on Computer Vision and Pattern Recognition (CVPR)*, 2023.
- [7] Chonghao Sima, Wenwen Tong, Tai Wang, Li Chen, Silei Wu, Hanming Deng, Yi Gu, Lewei Lu, Ping Luo, Dahua Lin, and Hongyang Li. Scene as occupancy, 2023.
- [8] Yuanhui Huang, Wenzhao Zheng, Yunpeng Zhang, Jie Zhou, and Jiwen Lu. Tri-perspective view for vision-based 3d semantic occupancy prediction. *arXiv preprint arXiv:2302.07817*, 2023.
- [9] Changhee Won, Jongbin Ryu, and Jongwoo Lim. End-to-end learning for omnidirectional stereo matching with uncertainty prior. *IEEE Transactions on Pattern Analysis and Machine Intelligence (PAMI)*, 2020.
- [10] Yanqin Jiang, Li Zhang, Zhenwei Miao, Xiatian Zhu, Jin Gao, Weiming Hu, and Yu-Gang Jiang. Polarformer: Multi-camera 3d object detection with polar transformers. In *AAAI*, 2023.
- [11] Shaoyu Chen, Xinggang Wang, Tianheng Cheng, Qian Zhang, Chang Huang, and Wenyu Liu. Polar parametrization for vision-based surround-view 3d detection. *arXiv:2206.10965*, 2022.
- [12] Yang Zhang, Zixiang Zhou, Philip David, Xiangyu Yue, Zerong Xi, Boqing Gong, and Hassan Foroosh. Polarnet: An improved grid representation for online lidar point clouds semantic segmentation. In *Proceedings of the IEEE/CVF Conference on Computer Vision and Pattern Recognition (CVPR)*, June 2020.
- [13] Xinge Zhu, Hui Zhou, Tai Wang, Fangzhou Hong, Yuexin Ma, Wei Li, Hongsheng Li, and Dahua Lin. Cylindrical and asymmetrical 3d convolution networks for lidar segmentation. *arXiv preprint arXiv:2011.10033*, 2020.
- [14] Alex Bewley, Pei Sun, Thomas Mensink, Dragomir Anguelov, and Cristian Sminchisescu. Range conditioned dilated convolutions for scale invariant 3d object detection. *CoRR*, abs/2005.09927, 2020.
- [15] J. Behley, M. Garbade, A. Milioto, J. Quenzel, S. Behnke, C. Stachniss, and J. Gall. SemanticKITTI: A Dataset for Semantic Scene Understanding of LiDAR Sequences. In *Proc. of the IEEE/CVF International Conf. on Computer Vision (ICCV)*, 2019.
- [16] Xiaoyu Tian, Tao Jiang, Longfei Yun, Yue Wang, Yilun Wang, and Hang Zhao. Occ3d: A large-scale 3d occupancy prediction benchmark for autonomous driving. *arXiv preprint arXiv:2304.14365*, 2023.
- [17] Xiaofeng Wang, Zheng Zhu, Wenbo Xu, Yunpeng Zhang, Yi Wei, Xu Chi, Yun Ye, Dalong Du, Jiwen Lu, and Xingang Wang. Openoccupancy: A large scale benchmark for surrounding semantic occupancy perception. *arXiv preprint arXiv:2303.03991*, 2023.
- [18] Jean-Emmanuel Deschaud, David Parreño Duque, Jean Pierre Richa, Santiago Velasco-Forero, Beatriz Marcotegui, and Francois Goulette. Paris-carla-3d: A real and synthetic outdoor point cloud dataset for challenging tasks in 3d mapping. *Remote. Sens.*, 13:4713, 2021.
- [19] Joey Wilson, Jingyu Song, Yuewei Fu, Arthur Zhang, Andrew Capodici, Paramsothy Jayakumar, Kira Barton, and Maani Ghaffari. Motionsc: Data set and network for real-time semantic mapping in dynamic environments, 2022.
- [20] Zhiqi Li, Wenhai Wang, Hongyang Li, Enze Xie, Chonghao Sima, Tong Lu, Yu Qiao, and Jifeng Dai. Bevformer: Learning bird's-eye-view representation from multi-camera images via spatiotemporal transformers. *arXiv*, 2022.
- [21] Chenyu Yang, Yuntao Chen, Haoifei Tian, Chenxin Tao, Xizhou Zhu, Zhaoxiang Zhang, Gao Huang, Hongyang Li, Y. Qiao, Lewei Lu, Jie Zhou, and Jifeng Dai. Bevformer v2: Adapting modern image backbones to bird's-eye-view recognition via perspective supervision. *ArXiv*, 2022.
- [22] Yingfei Liu, Tiancai Wang, Xiangyu Zhang, and Jian Sun. Petr: Position embedding transformation for multi-view 3d object detection. *arXiv preprint arXiv:2203.05625*, 2022.
- [23] Yingfei Liu, Junjie Yan, Fan Jia, Shuailin Li, Qi Gao, Tiancai Wang, Xiangyu Zhang, and Jian Sun. Petrv2: A unified framework for 3d perception from multi-camera images. *arXiv preprint arXiv:2206.01256*, 2022.
- [24] Lang Peng, Zhirong Chen, Zhangjie Fu, Pengpeng Liang, and Erkang Cheng. Bevsegformer: Bird's eye view semantic segmentation from arbitrary camera rigs, 2022.
- [25] Thomas Roddick and Roberto Cipolla. Predicting semantic map representations from images using pyramid occupancy networks, 2020.
- [26] Brady Zhou and Philipp Krähenbühl. Cross-view transformers for real-time map-view semantic segmentation. In *CVPR*, 2022.
- [27] Anh-Quan Cao and Raoul de Charette. Monoscene: Monocular 3d semantic scene completion. In *CVPR*, 2022.
- [28] Yi Wei, Lingqing Zhao, Wenzhao Zheng, Zheng Zhu, Jie Zhou, and Jiwen Lu. Surroundocc: Multi-camera 3d occupancy prediction for autonomous driving. *arXiv preprint arXiv:2303.09551*, 2023.
- [29] Qihang Ma, Xin Tan, Yanyun Qu, Lizhuang Ma, Zhizhong Zhang, and Yuan Xie. Cotr: Compact occupancy transformer for vision-based 3d occupancy prediction. *arXiv preprint arXiv:2312.01919*, 2023.
- [30] Simon Boeder, Fabian Gigengack, and Benjamin Risse. Occflownet: Towards self-supervised occupancy estimation via differentiable rendering and occupancy flow, 2024.
- [31] Junyi Ma, Xieyuanli Chen, Jiawei Huang, Jingyi Xu, Zhen Luo, Jintao Xu, Weihao Gu, Rui Ai, and Hesheng Wang. Cam4DOcc: Benchmark for Camera-Only 4D Occupancy Forecasting in Autonomous Driving Applications. In *Proc. of the IEEE/CVF Conf. on Computer Vision and Pattern Recognition (CVPR)*, 2024.
- [32] Yuqi Wang, Yuntao Chen, Xingyu Liao, Lue Fan, and Zhaoxiang Zhang. Panocc: Unified occupancy representation for camera-based 3d panoptic segmentation. *arXiv preprint arXiv:2306.10013*, 2023.
- [33] Haoyi Jiang, Tianheng Cheng, Naiyu Gao, Haoyang Zhang, Tianwei Lin, Wenyu Liu, and Xinggang Wang. Symphonize 3d semantic scene completion with contextual instance queries. *CVPR*, 2024.
- [34] Yunpeng Zhang, Zheng Zhu, and Dalong Du. Occformer: Dual-path transformer for vision-based 3d semantic occupancy prediction. *arXiv preprint arXiv:2304.05316*, 2023.
- [35] Luis Roldão, Raoul de Charette, and Anne Verroust-Blondet. Lmscnet: Lightweight multiscale 3d semantic completion. In *International Conference on 3D Vision (3DV)*, 2020.
- [36] Xu Yan, Jiantao Gao, Jie Li, Ruimao Zhang, Zhen Li, Rui Huang, and Shuguang Cui. Sparse single sweep lidar point cloud segmentation via learning contextual shape priors from scene completion. In *Proceedings of the AAAI Conference on Artificial Intelligence*, volume 35, pages 3101–3109, 2021.
- [37] Shuran Song, Fisher Yu, Andy Zeng, Angel X Chang, Manolis Savva, and Thomas Funkhouser. Semantic scene completion from a single depth image. *arXiv preprint arXiv:1611.08974*, 2016.
- [38] Sicheng Zuo, Wenzhao Zheng, Yuanhui Huang, Jie Zhou, and Jiwen Lu. Pointocc: Cylindrical tri-perspective view for point-based 3d semantic occupancy prediction. *arXiv preprint arXiv:2308.16896*, 2023.
- [39] Mingjie Pan, Jiaming Liu, Renrui Zhang, Peixiang Huang, Xiaoqi Li, Li Liu, and Shanghang Zhang. Renderocc: Vision-centric 3d occupancy prediction with 2d rendering supervision. *arXiv preprint arXiv:2309.09502*, 2023.
- [40] Yangyang Ding, Luying Huang, and Jiachen Zhong. Multi-scale occ: 4th place solution for cvpr 2023 3d occupancy prediction challenge, 2023.
- [41] Zhiqi Li, Zhiding Yu, David Austin, Mingsheng Fang, Shiyi Lan, Jan Kautz, and Jose M Alvarez. FB-OCC: 3D occupancy prediction based on forward-backward view transformation. *arXiv:2307.01492*, 2023.
- [42] Mingjie Pan, Li Liu, Jiaming Liu, Peixiang Huang, Longlong Wang, Shanghang Zhang, Shaoqing Xu, Zhiyi Lai, and Kuiyuan Yang.

Uniocc: Unifying vision-centric 3d occupancy prediction with geometric and semantic rendering, 2023.

- [43] Alexey Dosovitskiy, German Ros, Felipe Codevilla, Antonio Lopez, and Vladlen Koltun. CARLA: An open urban driving simulator. In *Proceedings of the 1st Annual Conference on Robot Learning*, pages 1–16, 2017.
- [44] Ming Li, Xiong Yang, Chaofan Wu, Jiaheng Li, Pinzhi Wang, Xuejiao Hu, Sidan Du, and Yang Li. Real-time multi-view omnidirectional depth estimation system for robots and autonomous driving on real scenes, 2024.
- [45] Yue Wang, Vitor Guizilini, Tianyuan Zhang, Yilun Wang, Hang Zhao, , and Justin M. Solomon. Detr3d: 3d object detection from multi-view images via 3d-to-2d queries. In *The Conference on Robot Learning (CoRL)*, 2021.
- [46] Haisong Liu, Yang Chen, Haiguang Wang, Zetong Yang, Tianyu Li, Jia Zeng, Li Chen, Hongyang Li, and Limin Wang. Fully sparse 3d occupancy prediction, 2024.